ACS OMEGA

Article

Cite This: ACS Omega 2019, 4, 95−103

http://pubs.acs.org/journal/acsodf

In Situ Cross-Linked Gel Polymer Electrolyte Membranes with Excellent Thermal Stability for Lithium Ion Batteries

Qin Xiao, Chun Deng, Qian Wang, Qiujing Zhang, Yong Yue, and Shijie Ren*

College of Polymer Science and Engineering, State Key Laboratory of Polymer Materials Engineering, Sichuan University, Chengdu 610065, P. R. China

Supporting Information

ABSTRACT: Novel gel polymer electrolyte membranes with excellent thermal stability are fabricated via a combination of physical blending and chemical cross-linking procedures. Precursor porous membranes made of poly(vinylidene fluoride) (PVDF) and polystyrene−poly(ethylene oxide)−polystyrene (PS−PEO−PS) triblock copolymer composites are prepared by a phase-inversion technique, and the gel polymer electrolyte membranes are finished by in situ hypercrosslinking of the PS segments in precursor membranes. The latter cross-linking procedure could consolidate pore configuration and thus greatly enhance the thermal stability of the obtained cross-linked composite membranes. The membranes with optimal PS/PEO ratios can retain reasonable porosity with little dimensional shrinkage at high temperatures up to 260 °C. Gel polymer electrolytes with these cross-linked membranes as matrices exhibit much higher ionic conductivities (up to 1.38×10^{-3} S cm^{-1} at room temperature) than those based on pure PVDF membranes. Li/LiFePO$_4$ half cells assembled with these gel polymer electrolytes exhibit good cycling performance and rate capability. These results indicate that the Friedel−Crafts reaction based hypercrosslinking is an efficient method to construct highly heat-resistant polymer electrolytes for lithium ion batteries, particularly advantageous in applications that require high-temperature usage.

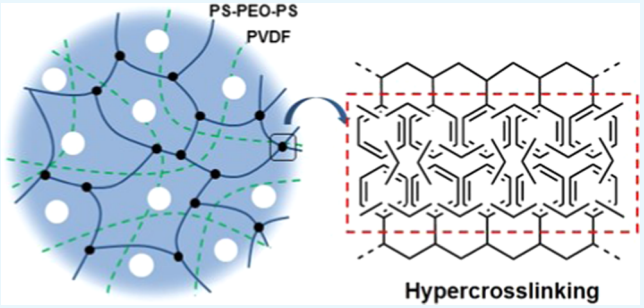

INTRODUCTION

With ever-growing demands for portable electronic devices, electric and hybrid vehicles and green energy storage, rechargeable lithium ion batteries (LIBs) with high energy density and long cycle life have widely been regarded as one of the most important energy storage systems.[1−3] However, rare but sometimes catastrophic safety accidents associated with the use of flammable liquid electrolytes and commercial polyolefin separators in LIBs have caused great concerns in the whole society.[4] Furthermore, although LIBs are usually used in ambient environment, it is also of great importance to develop LIBs that can be used at higher temperatures in specific areas such as oil drilling, mining, military, and aerospace electronics.[5] In recent decades, polymer electrolytes have attracted more and more attention because of their advantages over conventional liquid electrolytes, such as higher safety, mechanical flexibility, and better processability.[6,7]

At present, there are mainly two types of polymer electrolytes: solid polymer electrolytes (SPEs) and gel polymer electrolytes (GPEs). Solvent-free SPEs are normally formed by ion-conducting polymers complexed with lithium salts; however, low ionic conductivity (10^{-7}−10^{-5} S cm^{-1}) and poor compatibility with electrodes severely restrict their application in batteries. Compared with SPEs, GPEs formed by holding liquid electrolytes in polymer frameworks could essentially combine the advantages of both SPEs and liquid electrolytes, such as high ionic conductivity, good compatibility with electrodes, and reliable safety. A variety of polymers, such as poly(ethylene oxide) (PEO),[8,9] poly(methyl methacrylate),[10,11] poly(vinylidene fluoride) (PVDF),[12,13] and polyacrylonitrile,[14,15] have been used as matrices for GPEs due to their good interaction with lithium ions and polar liquid electrolytes. Among the above materials, PVDF as a polymer matrix for GPEs has attracted significant interest because of its high dielectric constant, good mechanical stability, and stable electrochemical performance. However, PVDF as a single component cannot hold enough amount of liquid electrolyte due to its semicrystalline structure, resulting in low ionic conductivity and electrolyte leakage issues of PVDF-based GPEs.[16]

To tackle these problems, linear and star-shaped PEO polymers were blended with PVDF, and porous GPEs based on these blends exhibited much higher ionic conductivity at room temperature due to their less crystalline structure and improved pore configuration.[12,13] However, PEO derivatives which tend to swell in polar liquid electrolytes could cause some dimensional and mechanical stability issues, and their low melting points also restrict the GPEs' usage at high

Received: September 3, 2018
Accepted: November 7, 2018
Published: January 2, 2019

DOI: 10.1021/acsomega.8b02255
ACS Omega 2019, 4, 95−103

temperature.[17] Cross-linking is an efficient method to enhance the mechanical and thermal stabilities of GPEs. GPEs based on semi-interpenetrating polymer networks composed of a PVDF matrix and PEO containing cross-linking moieties were prepared and exhibited much improved thermal stability and ionic conductivity.[18,19] However, conventional thermal or irradiation-induced cross-linking is highly energy consuming and might cause either unwanted side reactions or damage to the polymeric structures.[20] Therefore, it is still of great importance to develop more effective and milder cross-linking methods to prepare high-performance GPEs with good thermal stability.

Herein, we utilize a well-established cross-linking approach, which involves Friedel–Crafts reaction of aromatic molecules or polymers containing aromatic building blocks, to prepare a series of novel cross-linked GPE membranes that show excellent thermal stability. Previously, this method has been used to synthesize microporous hypercrosslinked polymers, which have been extensively used in gas storage and separation.[21−23] Briefly, precursor porous membranes composed of blends of PVDF and PS–PEO–PS triblock copolymers were prepared via a phase-inversion technique, followed by in situ hypercrosslinking of the polystyrene (PS) segments in the triblock copolymers, forming highly heat-resistant porous composite membranes. PEO segments in the triblock copolymers could improve the compatibility between PVDF and PS–PEO–PS copolymers in the blending and phase-inversion procedures, ensuring that the cross-linked PS–PEO–PS triblock copolymers could disperse uniformly in the PVDF matrix to form a semi-interpenetrating network, which helps in consolidating the pore configuration at elevated temperatures. The effect of PS chain length on thermal properties and electrochemical performances of the cross-linked gel polymer electrolytes (CPEs) was investigated, and it was found that with optimal PS/PEO ratios, the CPE membranes could retain reasonable porosity with little dimensional shrinkage at high temperatures up to 260 °C, which are indeed among the most thermally stable GPE membranes reported up to now and would be highly advantageous for LIBs used in harsh conditions. When conducted into test batteries, the CPEs exhibit much higher ionic conductivity (1.38×10^{-3} S cm^{-1}) and better electrochemical performances than those based on pure porous PVDF membranes.

RESULTS AND DISCUSSION

The synthetic route of the PS–PEO–PS triblock copolymers (SES-1–SES-5) is shown in Scheme S1 (Supporting Information). Using the same macroinitiator (MI) made from a poly(ethylene glycol) (PEG) polymer (M_n = 8000 g mol^{-1}), PS–PEO–PS triblock copolymers with different PS chain lengths SES-1–SES-5 were synthesized by atom transfer radical polymerization (ATRP) reaction with different MI/styrene feed ratios. The chemical structures of the Br–PEO–Br macroinitiator and PS–PEO–PS copolymers are verified by ^{1}H NMR (Figure S1) and Fourier transform infrared (FT-IR) spectra (Figure S2). Molecular weights and structural compositions of the PS–PEO–PS copolymers are summarized in Table 1, wherein the molecular weights of the PS segments were calculated from the integration ratios in the ^{1}H NMR spectra, and polymer dispersity indexes (PDIs) of the copolymers were determined by gel permeation chromatography (GPC) measurement. As shown in Table 1, the PS–PEO–PS copolymers possess molecular weights ranging from 11 000 to 56 000 g mol^{-1} with narrow molecular weight distributions and a wide range of PEO/PS composition ratios. The molecular weights of the copolymers determined by GPC exhibit the same trend as the results from NMR calculation (Table S1).

Table 1. Molecular Weights and Compositions of PS–PEO–PS Block Copolymers

samples	$M_{n,PEO}$[a] (g mol^{-1})	$M_{n,PS}$[b] (g mol^{-1})	$M_{n,total}$[c] (g mol^{-1})	wt % PEO/PS	PDI[d]
SES-1	8000	1560 × 2	11 120	71.9:28.1	1.26
SES-2	8000	2500 × 2	13 000	61.5:38.5	1.1
SES-3	8000	4800 × 2	17 600	45.5:54.5	1.23
SES-4	8000	10 400 × 2	28 800	27.7:72.3	1.23
SES-5	8000	24 250 × 2	56 500	16.5:83.5	1.33

[a]$M_{n,PEO}$ provided by the supplier. [b]$M_{n,PS}$ was determined by NMR. [c]$M_{n,total}$ was the sum of $M_{n,PEO}$ and $M_{n,PS}$. [d]PDI was obtained from GPC using tetrahydrofuran (THF) as the mobile phase and PS as the standard sample.

The fabrication process of the cross-linked polymer composite membranes is illustrated in Scheme 1. The precursor porous membranes were prepared by a phase-inversion technique using glycerin as the nonsolvent.[13,24] Thus, PVDF and PS–PEO–PS copolymers (w/w = 4:1) were completely dissolved to form a homogeneous solution in a mixture of *N*-methyl pyrrolidone (NMP) and glycerin (v/v = 10:1). During the evaporation of NMP at 90 °C, the glycerin molecules gathered into droplets, and uniformly dispersed in the solid-state membranes because of the strong interaction between PEO segments of the copolymers and glycerin. The porous precursor membranes were obtained after glycerin was completely removed at a higher temperature. Subsequently, the precursor porous membranes were in situ cross-linked in a solution of cross-linking agents containing formaldehyde dimethylacetal (FDA) as the cross-linker and $FeCl_3$ as the catalyst, during which PS segments in the PS–PEO–PS copolymers underwent a fast Friedel–Crafts alkylation reaction.[25] The cross-linked polymer composite membranes were obtained after extensive washing and drying under vacuum. There was little change in the shape and dimension of the membranes during the cross-linking process. The solubility of the precursor membranes and cross-linked membranes in common organic solvents such as tetrahydrofuran and NMP was studied. The precursor membranes without cross-linking could be completely dissolved, whereas for cross-linked membranes, there was always some insoluble residue that could be the hypercrosslinked PS–PEO–PS copolymers. For comparison, pure PVDF porous membranes without cross-linking were also manufactured by the phase-inversion technique.

The Brunauer–Emmett–Teller (BET) surface areas (SAs) of the cross-linked membranes were analyzed by nitrogen sorption analysis, and the results are summarized in Table 2. The BET surface area of the pure PVDF membrane was unmeasurable. With the introduction of PS–PEO–PS triblock copolymers, the cross-linked composite membranes of CPE-1, CPE-2, CPE-3, CPE-4, and CPE-5 exhibit BET surface areas of 18.3, 46.6, 38.2, 116.4, and 152.8 m^2 g^{-1}, respectively. It is clear that with an increase in the length of the PS segments in the copolymers, the BET surface areas of the resulting cross-linked membranes gradually increase, probably due to the

DOI: 10.1021/acsomega.8b02255
ACS Omega 2019, 4, 95−103

Scheme 1. Schematic Illustration for the Preparation and In Situ Cross-Linking Process of Heat-Resistant Porous Polymer Membranes

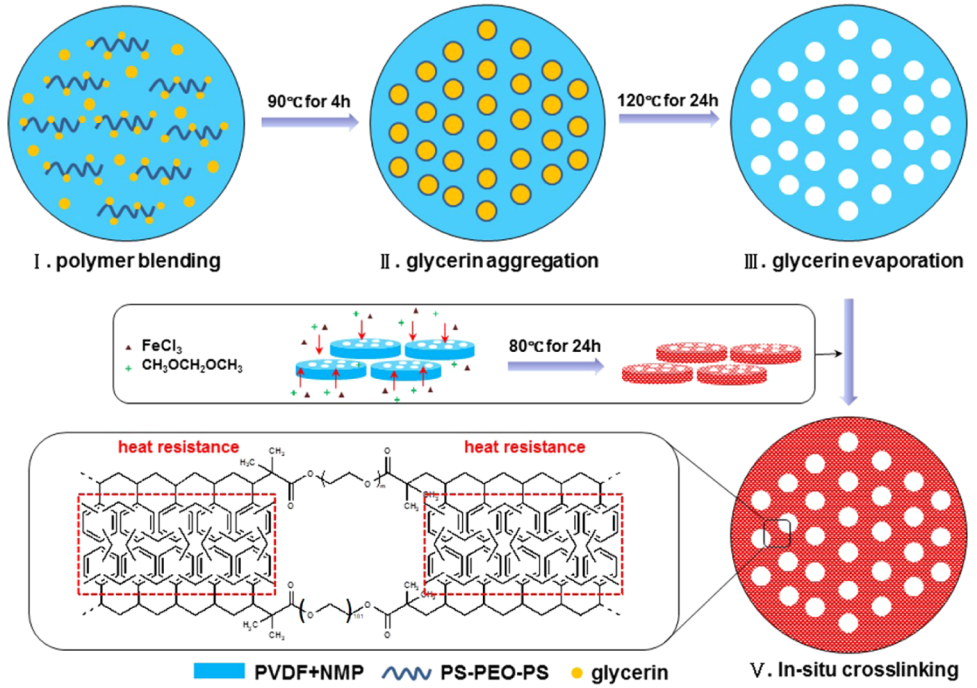

Table 2. SA_{BET}, Porosity, Electrolyte Uptake, Ionic Conductivity, and Activation Energy of Cross-Linked Gel Polymer Electrolyte Membranes Prepared with Different PS−PEO−PS Copolymers

samples	PVDF	CPE-1	CPE-2	CPE-3	CPE-4	CPE-5
SA_{BET}[a] ($m^2\ g^{-1}$)		18.3	46.6	38.2	116.4	152.8
porosity[b] (%)	50.0	63.7	64.4	63.6	58.3	49.8
electrolyte uptake[c] (%)	133	198	201	189	172	146
ionic conductivity[d] ($mS\ cm^{-1}$)	0.074	1.34	1.38	1.1	0.97	0.28
activation energy[e] ($kJ\ mol^{-1}$)	34.73	16.16	15.8	14.61	14.34	17.50

[a]Surface area (SA) calculated from nitrogen adsorption isotherms using the BET equation. [b]Porosity calculated from eq 1. [c]Electrolyte uptake was calculated according to eq 2. [d]The ionic conductivities were measured by electrochemical impedance spectroscopy. [e]Activation energy calculated from the equation $\sigma = \sigma_0 \exp(-E_a/RT)$.

production of micropores during the hypercrosslinking process.

Differential scanning calorimetry (DSC) (Figure S3) and thermogravimetry analysis (TGA) (Figure S4) measurements were conducted to understand the thermal properties of pure PVDF and the cross-linked membranes. All of the DSC curves show an endothermic peak at 160 °C, which corresponds to the melting of PVDF. TGA results show that the pure PVDF membrane starts to thermally degrade near 400 °C, and the weight loss of cross-linked membranes starts near 300 °C, indicating the thermal degradation of the copolymer.

The morphology of the pure PVDF membrane and the cross-linked membranes was investigated by scanning electron microscopy (Figures 1 and 2). From the surface and cross-sectional images, we can see that the membranes of CPEs have denser pore distribution than the pure PVDF membrane, especially for the membranes of CPE-1, CPE-2, and CPE-3, which possess relatively higher PEO/PS composition ratios. However, when the PS segments in the copolymers become larger, the pore distribution of membranes of CPE-4 and CPE-5 becomes sparser and the pore sizes increase. The possible reason is that phase separation between PVDF and PS−PEO−PS copolymers could occur upon further increasing the length of the PS chain in the added copolymers because of the incompatibility between PVDF and PS, leading to glycerin gathering in the PS−PEO−PS phase.[12,13,26]

Porosities of the porous membranes calculated by *n*-butanol absorption at room temperature are summarized in Table 2. The membranes prepared with PVDF/PS−PEO−PS composites exhibit higher porosities than pure PVDF, and the cross-linking procedure has no significant effect on the porosities (Table S2). The membranes of CPE-1, CPE-2, and CPE-3 have high porosities of about 64%, and the porosities of membranes of CPE-4 and CPE-5 decreased to 58.3 and 49.8% due to the phase separation between PVDF and PS−PEO−PS copolymers; the electrolyte uptake values of the porous membranes are also shown in Table 2, and the results are directly related to the porosity and affinity with liquid electrolytes. The cross-linked membrane of CPE-2 with the highest porosity (64.4%) and relatively high content of PEO segments shows the highest electrolyte uptake of 201%. To understand the effect of cross-linking on the thermal stability of the membranes, both the precursor membranes and cross-linked membranes were placed onto a hot plate for heat treatment at each temperature (from 120 to 300 °C) for 1 h and then cooled to room temperature for porosity measurement. The results are shown in Figure 3. With an increase in temperature, the porosities of all of the membranes decrease due to the melting of PVDF. When the temperature is increased to 200 °C, all of the precursor membranes without cross-linking are completely shut down, similar to the thermal behavior of pure PVDF (Figure S5); however, the cross-linked

DOI: 10.1021/acsomega.8b02255
ACS Omega 2019, 4, 95−103

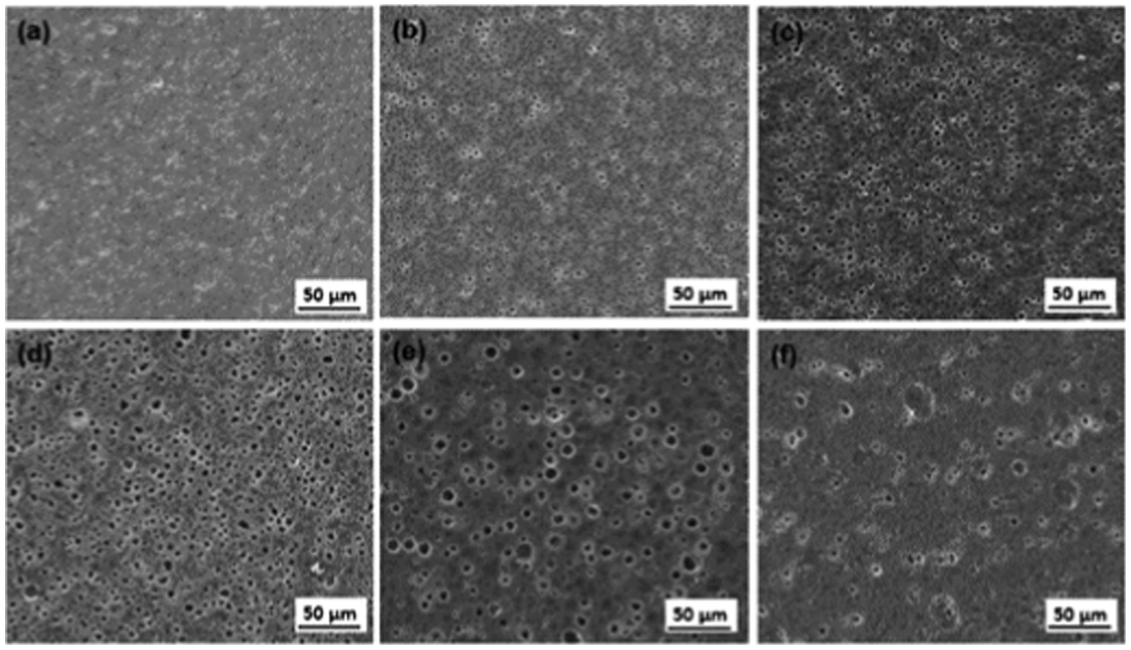

Figure 1. Surface morphology images of the porous membranes of (a) PVDF, (b) CPE-1, (c) CPE-2, (d) CPE-3, (e) CPE-4, and (f) CPE-5.

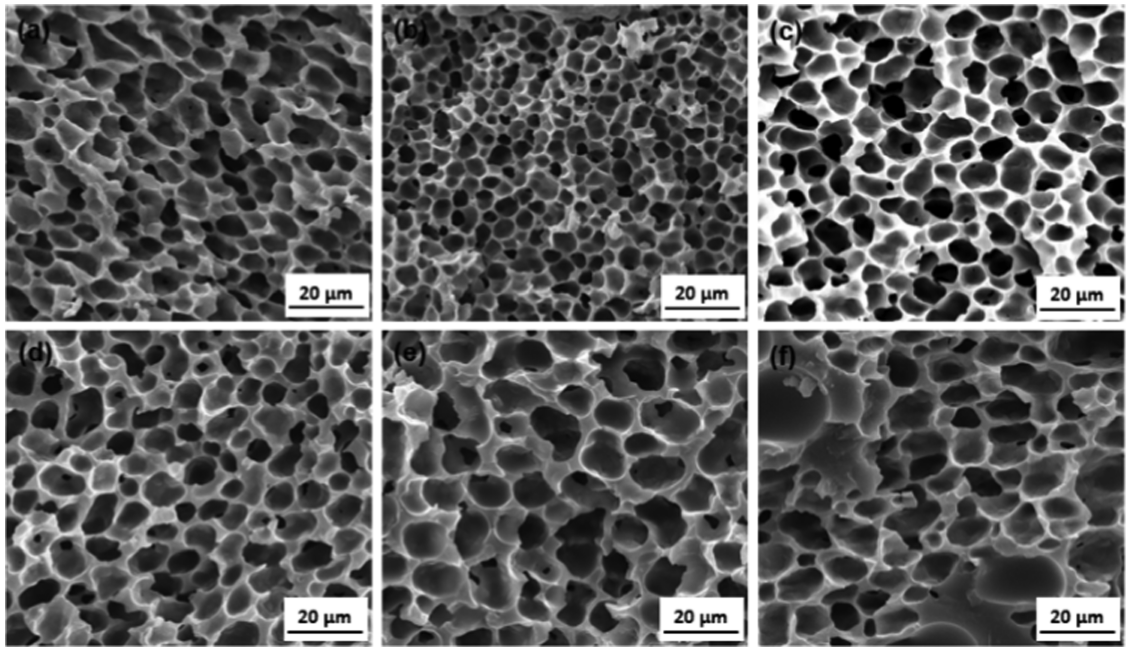

Figure 2. Cross-section images of the porous membranes of (a) PVDF, (b) CPE-1, (c) CPE-2, (d) CPE-3, (e) CPE-4, and (f) CPE-5.

membranes still showed variable porosities, from 10% of CPE-5 to over 35% of CPE-4. Further increasing the temperature to 260 °C, the membrane of CPE-4 still exhibits the highest porosity of close to 35%, which was comparable to the porosity of commercial polyolefin-based Li-ion battery separators at room temperature.[27] At an even higher temperature of 300 °C, the cross-linked membranes of CPE-2, CPE-3, and CPE-4 still show porosities of about 20%. The SEM images of the cross-linked membranes after heat treatment at 300 °C (Figures S6 and S7) also show that the polymer matrices of CPEs were partially melted, and the open pores still exist.

A polymer electrolyte must maintain its dimension at an elevated temperature to prevent direct contact between positive and negative electrodes. To evaluate thermal dimensional stability, thermal shrinkage behaviors of the cross-linked membranes, pure PVDF membrane, and commercial PP separator were recorded after placing the membranes onto a hot plate at 180 and 260 °C for 1 h, respectively (Figure 4). At 180 °C, the PP separator exhibited serious dimensional shrinkage, and the pure PVDF membrane was fully melt down and became transparent. In direct contrast, the cross-linked membranes of CPEs showed no obvious dimensional shrinkage. When the temperature reached up to 260 °C, the PP separator was thermally decomposed. The membranes of CPE-1 and CPE-2 exhibited a certain degree of thermal shrinkage, and there was still little dimensional shrinkage for

DOI: 10.1021/acsomega.8b02255
ACS Omega 2019, 4, 95−103

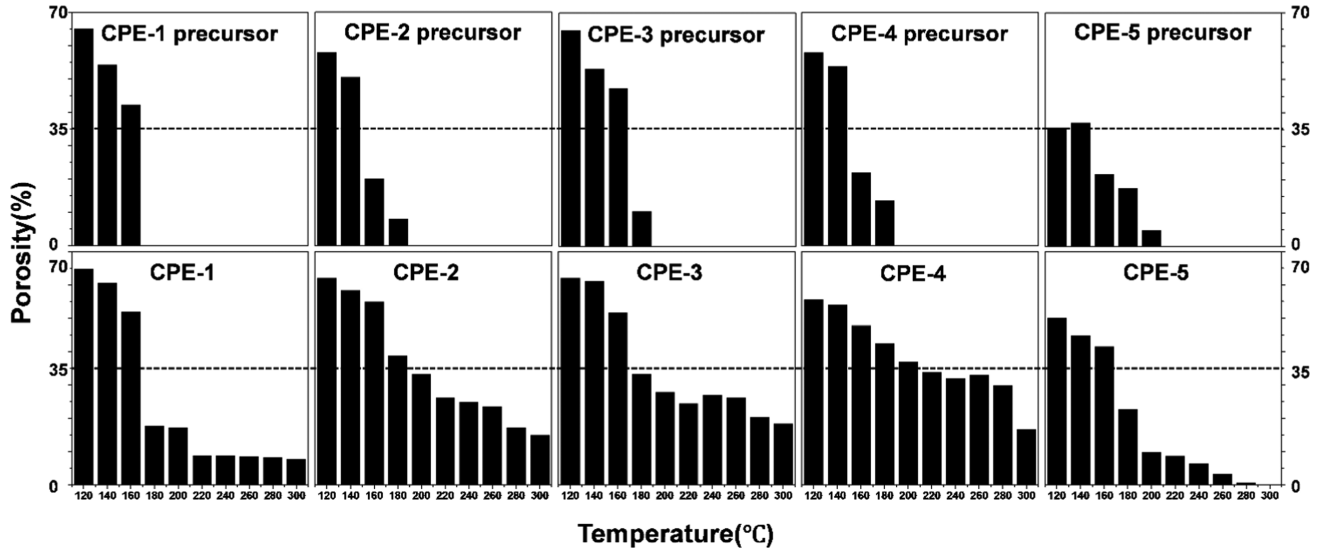

Figure 3. Porosities of the precursor membranes (top half) and cross-linked membranes (bottom half) of CPE-1, CPE-2, CPE-3, CPE-4, and CPE-5 under heat treatment at different temperatures from 120 to 300 °C.

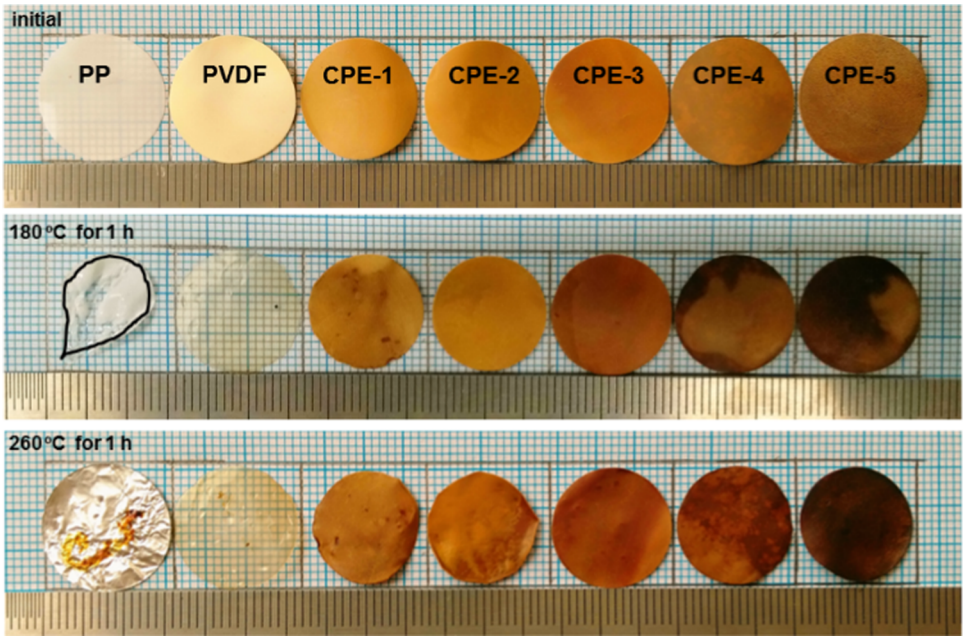

Figure 4. Photographs of the commercial PP separator and membranes of pure PVDF, CPE-1, CPE-2, CPE-3, CPE-4, and CPE-5 before and after thermal exposure at 180 and 260 °C for 1 h (When the temperature reached 260 °C, the decomposed PP separator on the bottom left was completely stuck on the aluminum foil and cannot be removed.).

cross-linked membranes of CPE-3, CPE-4, and CPE-5. It is clear that the greater the degree of cross-linking, the better the thermal dimensional stability. This, combined with the sustained porosity of CPE membranes at high temperature, shows that the cross-linking procedure could consolidate pore configuration and thus greatly enhance the thermal stability of the obtained cross-linked composite membranes. There are substantial research interest and market demand for electrical energy storage that operates at high temperature for use in the oil and gas (60−200 °C) industry, military, aviation, aerospace, and the automotive and electric vehicle sectors (up to 300 °C).[5] We believe that the CPE membranes with excellent thermal dimensional stability and stable pore configuration at elevated temperatures show great potential in high-temperature electrical energy storage.[7]

Alternating current (AC) impedance spectroscopy was used to measure the ion conductivities of the PVDF porous membrane and the CPEs. Figure 5a shows the Nyquist plots of CPEs at room temperature. It can be seen that the bulk impedance of pure PVDF is the largest, and the impedance of the CPEs increases when the PS chain length is elevated. The ion conductivities of pure PVDF and CPEs at room temperature were calculated and are shown in Table 2. Pure PVDF has the lowest ion conductivity of 0.074×10^{-3} S cm^{-1} due to its low porosity and semicrystalline structure, which is not favorable for lithium ion transport.[18] CPE-1 and CPE-2 have similar ion conductivities of 1.34×10^{-3} and 1.38×10^{-3}

DOI: 10.1021/acsomega.8b02255
ACS Omega 2019, 4, 95−103

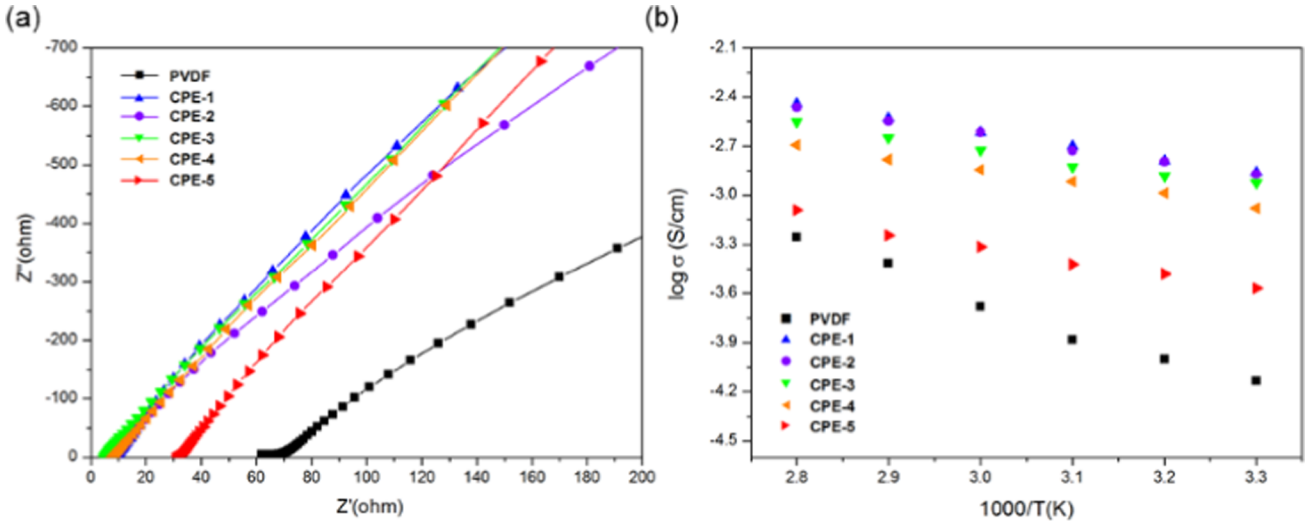

Figure 5. (a) Nyquist plots at room temperature, and (b) temperature dependence of ionic conductivity for PVDF, CPE-1, CPE-2, CPE-3, CPE-4, and CPE-5.

S cm^{-1}, which agree with their almost the same porosity and electrolyte uptake. When the PS chain length further increases, the ion conductivities of CPE-3, CPE-4, and CPE-5 decline gradually due to their decreasing porosity and less content of PEO segments. Figure 5b shows the dependence of ionic conductivity on temperature ranging from 30 to 80 °C.

All of the curves of CPEs are nearly linear, and the ion conductivities increase with an increase in temperature because of the stronger lithium ion mobility at a higher temperature, which presents typical Arrhenius conductive behavior. The activation energy for ion transportation of the CPEs can be calculated from the equation $\sigma = \sigma_0 \exp(-E_a/RT)$, where σ is the measured ion conductivity, and σ_0 and R are the pre-exponential factor and gas constant, respectively. The slope was obtained from the $\log \sigma - 1000/T$ curves in Figure 5b. The E_a values for pure PVDF and CPEs are shown in Table 2. The E_a value of pure PVDF (34.73 kJ mol^{-1}) is much higher than that of CPEs (14−17 kJ mol^{-1}) because of its low porosity and semicrystalline structure.

The linear sweep voltammetry (LSV) test was carried out to evaluate the electrochemical stability window of the CPEs. As shown in Figure 6, there is no obvious oxidation peak in the wide potential range from 0 to 5.0 V (vs Li/Li^+),

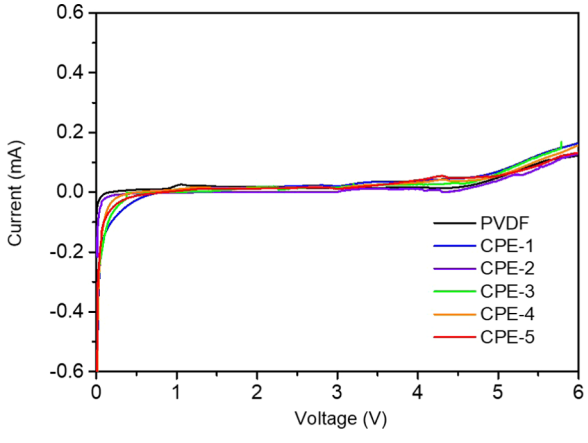

Figure 6. Linear sweep voltammetry curves for PVDF, CPE-1, CPE-2, CPE-3, CPE-4, and CPE-5.

demonstrating that the CPEs have an electrochemical stability window of 5.0 V (vs Li/Li^+), and no apparent difference is observed in the electrochemical stability among different CPEs.

The charge−discharge performances of lithium ion batteries with different CPEs as the gel electrolytes were evaluated by using $LiFePO_4$ as the cathode and Li metal as the reference electrode. Cycling performances of the cells are shown in Figure 7a. The cells assembled with pure PVDF with a semicrystalline structure and low porosity exhibit the lowest initial discharge specific capacity of 125.3 mA h g^{-1}. The batteries containing CPE-1, CPE-2, CPE-3, and CPE-4 show high initial discharge specific capacities of 145.3, 138.4, 133.8, and 140.4 mA h g^{-1} at 0.1C, respectively. However, the discharge specific capacity of the cell containing CPE-5 (128.2 mA h g^{-1}) is relatively lower, which may be caused by its low porosity and electrolyte uptake.[28] After 40 cycles, the cell containing pure PVDF shows a capacity retention of 78.1% and the discharge capacity retention values of cells containing CPE-1, CPE-2, CPE-3, CPE-4, and CPE-5 are 95.5, 100, 97.5, 90.7, and 87.7%, respectively. Capacity retention of the cells is determined by the ion conductivity and affinity with liquid electrolyte, which allows better electrolyte retention during cycling.[12,29,30] With the addition of PS−PEO−PS copolymers, which enhances the ionic conductivity and the affinity with liquid electrolytes, the CPEs show better cycling performances than pure PVDF. Among them, CPE-1, CPE-2, and CPE-3 exhibited superior capacity retention, and when the PS chain length of the added copolymers further increases, the ionic conductivities and the content of PEO segments in the CPEs decrease, resulting in lower capacity retention. As shown in Figure S8, the overpotentials of cells assembled with CPE-1−CPE-4 are smaller than that of the cell assembled with PVDF, indicating a smaller polarization effect. The highly reversible capacities between charge and discharge processes for cells assembled with CPE-1−CPE-3 indicate the good stability of the electrode/electrolyte interfaces. Among them, CPE-2 with a low overpotential and a highly reversible capacity is expected to be a good candidate for gel polymer electrolytes.

Although the discharge capacity of the cells decreases when the discharge rate increases from 0.2C to 2C due to the

DOI: 10.1021/acsomega.8b02255
ACS Omega 2019, 4, 95−103

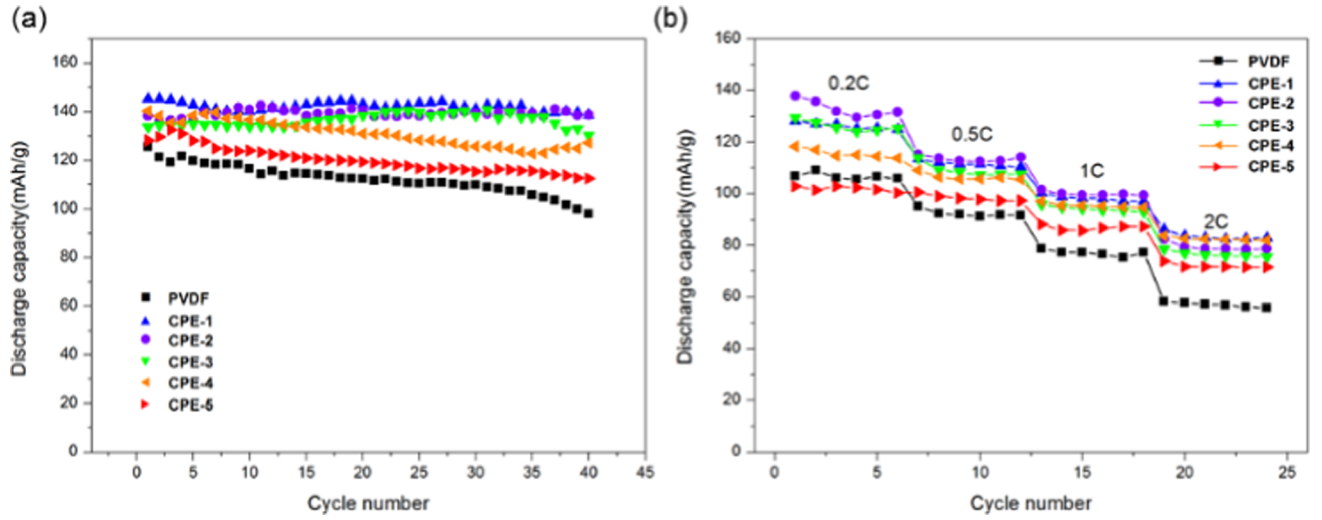

Figure 7. (a) Cycling performance and (b) C-rate performance of Li/$LiFePO_4$ batteries assembled with PVDF, CPE-1, CPE-2, CPE-3, CPE-4, and CPE-5.

sluggish Li ion diffusion kinetics at high rates, the cells assembled with CPE-1 and CPE-2 show relatively higher discharge capacity than others at each rate, as shown in Figure 7b, indicating that they have better rate properties.[31] The cell using CPE-2 exhibits capacities of 131.6, 114.4, 99.1, and 79.2 mA h g^{-1} at rates of 0.2C, 0.5C, 1C, and 2C, and the capacities at each rate of the cell containing pure PVDF are 106.8, 95.1, 78.8, and 58.3 mA h g^{-1}, respectively. When the current density increases from 0.2C to 2C, the capacity retention values of the cells containing pure PVDF and CPE-2 were 54.6 and 60.0%, respectively. The better rate performances of the cells assembled with CPEs than pure PVDF might benefit from higher ion conductivities and better affinity with the liquid electrolyte, which allows faster transportation of lithium ions at high charge−discharge rates.[30,32] The first cycle charge−discharge curves of the cells at different C-rates are shown in Figure S9. It also shows that the cells assembled with CPEs have higher initial efficiency than PVDF at each rate. In addition, with an increase in the C-rates from 0.2C to 2C, the charging plateau increases, whereas the discharging plateau continuously decreases, indicating the increase in battery resistance and polarization. Compared with the cell assembled with pure PVDF, CPEs exhibit relatively smaller voltage platform changes, indicating better rate performances of the composite polymer electrolytes.

CONCLUSIONS

In summary, novel cross-linked gel polymer electrolytes based on PVDF and PS−PEO−PS triblock copolymers were prepared by combining the phase-inversion technique and the in situ hypercrosslinking procedure. The as-prepared membranes exhibit high porosity and uniform pore size, and the cross-linking procedure consolidates pore configuration and thus greatly enhances the thermal stability of the obtained composite membranes. The membranes with optimal PS/PEO ratios could retain reasonable porosity with little dimensional shrinkage at high temperatures up to 260 °C, which are indeed among the most thermally stable GPE membranes reported up to now. GPEs with these cross-linked membranes as matrices exhibit much higher ionic conductivities (up to 1.38×10^{-3} S cm^{-1} at room temperature) than those based on pure PVDF membranes. Moreover, half cells assembled with CPEs show much better cycling performances and rate capability than pure PVDF. These results indicate that Friedel−Crafts reaction-based hypercrosslinking is an efficient method to construct highly heat-resistant gel polymer electrolytes for lithium ion batteries, particularly advantageous in applications that require high-temperature usage.

EXPERIMENTAL SECTION

Materials. Poly(ethylene glycol) (PEG, M_n = 8000 g mol^{-1}, Sigma-Aldrich), PVDF (HSV900, Kynar), *N,N,N′,N″,N″*-pentamethyldiethylenetriamine (PMDETA, 99%, Acros), *α*-bromoisobutyryl bromide (98%, Sigma-Aldrich), triethylamine, formaldehyde dimethylacetal (FDA), and anhydrous $FeCl_3$ were used as received. CuBr was washed with acetic acid before use. Tetrahydrofuran (THF), dichloromethane, and 1,4-dioxane were dried before use. Styrene was purified by distillation at reduced pressure. 1 M $LiPF_6$−ethylene carbonate/dimethyl carbonate/ethylmethyl carbonate (w/w/w = 1:1:1) liquid electrolyte, $LiFePO_4$ powder (battery-grade), and acetylene black were purchased from Shanxi Lizhiyuan Battery Materials Co. Ltd.

Preparation of the Triblock Copolymers. The PS−PEO−PS triblock copolymers were synthesized by atom transfer radical polymerization (ATRP) using the Br−PEO−Br macroinitiator (MI) according to a literature procedure.[33] A series of copolymers were synthesized with the MI/CuBr/PMDETA/St molar ratios of 1:2:3:30, 1:2:3:50, 1:2:3:100, 1:2:3:200, and 1:2:3:460 and were labeled as SES-1, SES-2, SES-3, SES-4, and SES-5, respectively.

Preparation of Precursor Porous Membranes. PVDF/PS−PEO−PS porous membranes were prepared by a phase-inversion technique. 4 g of PVDF and 1 g of PS−PEO−PS copolymer were dissolved in a mixture of NMP (solvent, 35 mL) and glycerin (non-solvent, 3.5 mL). The mixture was heated under vigorous stirring at 80 °C for 24 h until a homogeneous solution was obtained. After being cooled to room temperature, the solution was poured into a Petri dish and placed on a hot plate at 90 °C for 4 h to remove NMP, and then placed in a vacuum oven at 120 °C for 24 h to remove the glycerin. The free-standing membranes were cut into circular pieces (d = 16 mm) before use.

DOI: 10.1021/acsomega.8b02255
ACS Omega 2019, 4, 95−103

Preparation of Cross-Linked Gel Polymer Electrolytes. $FeCl_3$ (4.875 g), FDA (2.65 mL), and 20 mL of 1,2-dichloroethane were added to a flask and stirred in an ice bath until it is completely mixed. PVDF/PS−PEO−PS (500 mg) precursor membranes were added to the mixture and then heated at 80 °C for 24 h without stirring. At the end of the reaction, the obtained membranes were washed with acetone, 1 M hydrochloric acid, and deionized water successively, purified by a Soxhlet extractor with methanol for 24 h, and finally dried in a vacuum oven at 60 °C for 24 h. The resulting membranes were immersed in a liquid electrolyte solution in a glove box before being conducted into lithium batteries. For convenience, the in situ cross-linked gel polymer electrolytes are labeled as CPE-1, CPE-2, CPE-3, CPE-4, and CPE-5, corresponding to the samples prepared with SES-1, SES-2, SES-3, SES-4, and SES-5, respectively.

Characterization. NMR (Bruker 400 MHz) and Fourier transform infrared spectroscopy (FT-IR, Nicolet 6700) were used to examine the chemical structures of the copolymers. Polymer dispersity indexes (PDIs) of the copolymers were measured by gel permeation chromatography (GPC, Waters 2695) using THF as the mobile phase and PS as the standard sample. Scanning electron microscopy (SEM, JEOL JSM-7500F) was used to characterize the morphology of the CPE membranes. Specific surface areas of the samples were measured by a gas adsorption analyzer (Belsorp-Max). The thermal properties of the membranes were evaluated by differential scanning calorimetry (DSC, Perkin Elmer DSC 8500) and thermogravimetry analysis (TGA, Perkin Elmer STA 6000) under a nitrogen atmosphere with a heating rate of 10 °C min^{-1}.

To measure porosity, the membranes were immersed into *n*-butanol for 4 h until equilibrium was achieved at room temperature. The porosity (P) was calculated according to the following equation

$$P\ (\%) = \frac{m_1 - m_0}{\rho V_0} \times 100\% \quad (1)$$

where m_1 and m_0 are the weights of the membrane saturated with *n*-butanol and dry membrane, respectively, ρ is the density of *n*-butanol, and V_0 is the geometric volume of the membrane.

Electrolyte uptake of the membranes was calculated according to the following equation

$$U\ (\%) = \frac{W_1 - W_0}{W_0} \times 100 \quad (2)$$

where W_0 is the weight of dry membrane, and W_1 is the weight of the membrane after absorbing the liquid electrolyte.

Ionic conductivity of the CPEs was determined by AC impedance spectroscopy using an electrochemical workstation system (CHI660e, Shanghai Chenhua Instruments Co., Ltd., China) at an amplitude of 10 mV over a frequency range from 1 Hz to 100 kHz. By sandwiching the polymer electrolytes between two stainless steel electrodes, the bulk impedance (R_b) could be measured. The ion conductivity (σ) can be calculated using the following equation

$$\sigma = \frac{d}{R_b \times S} \quad (3)$$

where d is the thickness of the polymer electrolytes, and S is the effective area between electrolytes and stainless steel blocking electrodes.

The electrochemical stability window of CPEs was measured by the linear sweep voltammetry (LSV) at room temperature using a two-electrode cell with a stainless steel working electrode and a lithium foil reference electrode. The measurement was carried out between 0 and 6.0 V (vs Li/Li^+) at a scan rate of 1 mV s^{-1}.

The CPEs were sandwiched between the $LiFePO_4$ cathode ($LiFePO_4$/acetylene black/PVDF, 8:1:1, w/w/w) and the lithium metal anode in a coin cell to analyze their battery performance, including the charge−discharge curve, cycling property, and C-rate capability. The charge−discharge curve was obtained at 0.1C, 0.2C, 0.5C, 1C, and 2C between 2.5 and 4.2 V. The cycling property of the cells at room temperature was conducted in a Land battery test system (CT 2001A, Wuhan Land Electronic Co. Ltd.) at a current density of 0.1C between 2.5 and 4.2 V. The rate capability was tested under current densities of 0.2C, 0.5C, 1C, and 2C for six cycles at each rate at room temperature. All of the cells were assembled in an argon-filled glove box with oxygen and moisture level <1 ppm.

■ ASSOCIATED CONTENT

Supporting Information

The Supporting Information is available free of charge on the ACS Publications website at DOI: 10.1021/acsomega.8b02255.

Synthesis strategy of the PS−PEO−PS triblock copolymer (Scheme S1), ^1H NMR spectra of the samples (Figure S1), molecular weights of PS−PEO−PS block copolymers (Table S1), FT-IR spectra of the samples (Figure S2), porosities of the precursor membranes and cross-linked membranes of CPEs (Table S2), DSC curves of the membranes of PVDF and CPEs (Figure S3), TGA curves of the membranes of PVDF and CPEs (Figure S4), porosities of the pure PVDF membrane under heat treatment at different temperatures (Figure S5), surface morphology images of the cross-linked membranes of CPEs after heat treatment at 300 °C (Figure S6), cross-sectional morphology images of the cross-linked membranes of CPEs after heat treatment at 300 °C (Figure S7), charge−discharge curves of the cells at the rate of 0.1C (Figure S8), and initial charge−discharge curves of the cells at each rate (0.2C, 0.5C, 1C, and 2C) (Figure S9) (PDF)

■ AUTHOR INFORMATION

Corresponding Author

*E-mail: rensj@scu.edu.cn.

ORCID

Shijie Ren: 0000-0002-7562-8666

Author Contributions

The manuscript was written through the contributions of all authors. All authors have given approval to the final version of the manuscript.

Notes

The authors declare no competing financial interest.

DOI: 10.1021/acsomega.8b02255
ACS Omega 2019, 4, 95−103

■ ACKNOWLEDGMENTS

This work is financially supported by the Natural Science Foundation of China (21574087, 21404074), Science and Technology Department of Sichuan province (2015JY0143), and China Postdoctoral Science Foundation (2015M570785).

■ REFERENCES

(1) Tarascon, J. M.; Armand, M. Issues and challenges facing rechargeable lithium batteries. *Nature* **2001**, *414*, 359−367.
(2) Blomgren, G. E. The Development and Future of Lithium Ion Batteries. *J. Electrochem. Soc.* **2017**, *164*, A5019−A5025.
(3) Goodenough, J. B.; Park, K. S. The Li-Ion Rechargeable Battery: A Perspective. *J. Am. Chem. Soc.* **2013**, *135*, 1167−1176.
(4) Wang, Q.; Ping, P.; Zhao, X.; Chu, G.; Sun, J.; Chen, C. Thermal runaway caused fire and explosion of lithium ion battery. *J. Power Sources* **2012**, *208*, 210−224.
(5) Lin, X.; Salari, M.; Arava, L. M.; Ajayan, P. M.; Grinstaff, M. W. High temperature electrical energy storage: advances, challenges, and frontiers. *Chem. Soc. Rev.* **2016**, *45*, 5848−5887.
(6) Porcarelli, L.; Shaplov, A. S.; Bella, F.; Nair, J. R.; Mecerreyes, D.; Gerbaldi, C. Single-Ion Conducting Polymer Electrolytes for Lithium Metal Polymer Batteries that Operate at Ambient Temperature. *ACS Energy Lett.* **2016**, *1*, 678−682.
(7) Long, L.; Wang, S.; Xiao, M.; Meng, Y. Polymer electrolytes for lithium polymer batteries. *J. Mater. Chem. A* **2016**, *4*, 10038−10069.
(8) Egashira, M.; Todo, H.; Yoshimoto, N.; Morita, M. Lithium ion conduction in ionic liquid-based gel polymer electrolyte. *J. Power Sources* **2008**, *178*, 729−735.
(9) Wang, S. H.; Hou, S. S.; Kuo, P. L.; Teng, H. Poly(ethylene oxide)-co-Poly(propylene oxide)-Based Gel Electrolyte with High Ionic Conductivity and Mechanical Integrity for Lithium-Ion Batteries. *ACS Appl. Mater. Interfaces* **2013**, *5*, 8477−8485.
(10) Sharma, J.; Sekhon, S. Nanodispersed polymer gel electrolytes: Conductivity modification with the addition of PMMA and fumed silica. *Solid State Ionics* **2007**, *178*, 439−445.
(11) Liao, Y. H.; Zhou, D. Y.; Rao, M. M.; Li, W. S.; Cai, Z. P.; Liang, Y.; Tan, C. L. Self-supported poly(methyl methacrylate−acrylonitrile−vinyl acetate)-based gel electrolyte for lithium ion battery. *J. Power Sources* **2009**, *189*, 139−144.
(12) Deng, F.; Wang, X.; He, D.; Hu, J.; Gong, C.; Ye, Y. S.; Xie, X.; Xue, Z. Microporous polymer electrolyte based on PVDF/PEO star polymer blends for lithium ion batteries. *J. Membr. Sci.* **2015**, *491*, 82−89.
(13) Xi, J.; Qiu, X.; Li, J.; Tang, X.; Zhu, W.; Chen, L. PVDF−PEO blends based microporous polymer electrolyte: Effect of PEO on pore configurations and ionic conductivity. *J. Power Sources* **2006**, *157*, 501−506.
(14) Wang, Q.; Song, W.-L.; Fan, L. Z.; Shi, Q. Effect of polyacrylonitrile on triethylene glycol diacetate-2-propenoicacid butyl ester gel polymer electrolytes with interpenetrating crosslinked network for flexible lithium ion batteries. *J. Power Sources* **2015**, *295*, 139−148.
(15) Raghavan, P.; Manuel, J.; Zhao, X.; Kim, D. S.; Ahn, J. H.; Nah, C. Preparation and electrochemical characterization of gel polymer electrolyte based on electrospun polyacrylonitrile nonwoven membranes for lithium batteries. *J. Power Sources* **2011**, *196*, 6742−6749.
(16) Zhang, H.; Ma, X.; Lin, C.; Zhu, B. Gel polymer electrolyte-based on PVDF/fluorinated amphiphilic copolymer blends for high performance lithium-ion batteries. *RSC Adv.* **2014**, *4*, 33713−33719.
(17) Kuo, P. L.; Wu, C. A.; Lu, C. Y.; Tsao, C. H.; Hsu, C. H.; Hou, S. S. High Performance of Transferring Lithium Ion for Polyacrylonitrile-Interpenetrating Crosslinked Polyoxyethylene Network as Gel Polymer Electrolyte. *ACS Appl. Mater. Interfaces* **2014**, *6*, 3156−3162.
(18) Shim, J.; Lee, J. S.; Lee, J. H.; Kim, H. J.; Lee, J. C. Gel Polymer Electrolytes Containing Anion-Trapping Boron Moieties for Lithium-Ion Battery Applications. *ACS Appl. Mater. Interfaces* **2016**, *8*, 27740−27752.
(19) Lu, Q.; Yang, J.; Lu, W.; Wang, J.; Nuli, Y. Advanced semi-interpenetrating polymer network gel electrolyte for rechargeable lithium batteries. *Electrochim. Acta* **2015**, *152*, 489−495.
(20) Hwang, S. S.; Cho, C. G.; Kim, H. Room temperature cross-linkable gel polymer electrolytes for lithium ion batteries by in situ cationic polymerization of divinyl ether. *Electrochem. Commun.* **2010**, *12*, 916−919.
(21) Li, B.; Gong, R.; Wang, W.; Huang, X.; Zhang, W.; Li, H.; Hu, C.; Tan, B. A New Strategy to Microporous Polymers: Knitting Rigid Aromatic Building Blocks by External Cross-Linker. *Macromolecules* **2011**, *44*, 2410−2414.
(22) Wang, K.; Huang, L.; Razzaque, S.; Jin, S.; Tan, B. Fabrication of Hollow Microporous Carbon Spheres from Hyper-Crosslinked Microporous Polymers. *Small* **2016**, *12*, 3134−3142.
(23) Li, B.; Yang, X.; Xia, L.; Majeed, M. I.; Tan, B. Hollow Microporous Organic Capsules. *Sci. Rep.* **2013**, *3*, No. 2128.
(24) Zhu, Y. S.; Xiao, S. Y.; Li, M. X.; Chang, Z.; Wang, F. X.; Gao, J.; Wu, Y. P. Natural macromolecule based carboxymethyl cellulose as a gel polymer electrolyte with adjustable porosity for lithium ion batteries. *J. Power Sources* **2015**, *288*, 368−375.
(25) Qiao, Z. A.; Chai, S. H.; Nelson, K.; Bi, Z.; Chen, J.; Mahurin, S. M.; Zhu, X.; Dai, S. Polymeric molecular sieve membranes via in situ cross-linking of non-porous polymer membrane templates. *Nat. Commun.* **2014**, *5*, No. 3705.
(26) Xiao, Q.; Wang, X.; Li, W.; Li, Z.; Zhang, T.; Zhang, H. Macroporous polymer electrolytes based on PVDF/PEO-b-PMMA block copolymer blends for rechargeable lithium ion battery. *J. Membr. Sci.* **2009**, *334*, 117−122.
(27) Zhang, S. S. A review on the separators of liquid electrolyte Li-ion batteries. *J. Power Sources* **2007**, *164*, 351−364.
(28) Yanilmaz, M.; Lu, Y.; Zhu, J.; Zhang, X. Silica/polyacrylonitrile hybrid nanofiber membrane separators via sol-gel and electrospinning techniques for lithium-ion batteries. *J. Power Sources* **2016**, *313*, 205−212.
(29) Zhai, Y.; Wang, N.; Mao, X.; Si, Y.; Yu, J.; Al-Deyab, S. S.; El-Newehy, M.; Ding, B. Sandwich-structured PVdF/PMIA/PVdF nanofibrous separators with robust mechanical strength and thermal stability for lithium ion batteries. *J. Mater. Chem. A* **2014**, *2*, 14511.
(30) Shi, J.; Hu, H.; Xia, Y.; Liu, Y.; Liu, Z. Polyimide matrix-enhanced cross-linked gel separator with three-dimensional heat-resistance skeleton for high-safety and high-power lithium ion batteries. *J. Mater. Chem. A* **2014**, *2*, 9134−9141.
(31) Quartarone, E.; Mustarelli, P. Electrolytes for solid-state lithium rechargeable batteries: recent advances and perspectives. *Chem. Soc. Rev.* **2011**, *40*, 2525−2540.
(32) Liu, K.; Liu, M.; Cheng, J.; Dong, S.; Wang, C.; Wang, Q.; Zhou, X.; Sun, H.; Chen, X.; Cui, G. Novel cellulose/polyurethane composite gel polymer electrolyte for high performance lithium batteries. *Electrochim. Acta* **2016**, *215*, 261−266.
(33) Beaudoin, E.; Phan, T. N.; Robinet, M.; Denoyel, R.; Davidson, P.; Bertin, D.; Bouchet, R. Effect of Interfaces on the Melting of PEO Confined in Triblock PS-b-PEO-b-PS Copolymers. *Langmuir* **2013**, *29*, 10874−10880.

DOI: 10.1021/acsomega.8b02255
ACS Omega 2019, 4, 95−103